Cement and Concrete Research 140 (2021) 106307

Contents lists available at ScienceDirect

Cement and Concrete Research

journal homepage: www.elsevier.com/locate/cemconres

The reaction between metakaolin and limestone and its effect in porosity refinement and mechanical properties

Franco Zunino *, Karen Scrivener

Laboratory of Construction Materials, EPFL STI IMX LMC, École Polytechnique Fédérale de Lausanne, 1015 Lausanne, Switzerland

ARTICLE INFO

Keywords:
A hydration
A kinetics
B calcium-silicate-hydrate (C-S-H)
B hydration products
B microstructure

ABSTRACT

In limestone calcined clay cements (LC^3), more hemicarboaluminate and monocarboaluminate is observed, as compared to other blended cements, from the reaction of metakaolin with limestone. In this study, it is shown that the formation of these carboaluminate phases, predominantly occurs during a "third" hydration peak, after the main alite and aluminate peaks. The influence of the metakaolin content, level of sulfate addition and the water to binder ratio on the position and magnitude of this peak were investigated. This precipitation of hemi and monocarboaluminate has a significant effect on porosity refinement and strength development. It was also observed that alumina from metakaolin can contribute to the precipitation of ettringite if sufficient sulfate is available.

1. Introduction

Cement is accountable for about 6% of the anthropogenic CO_2 emissions worldwide [1]. The most effective strategy to reduce the carbon footprint of the cement industry on a worldwide scale is to reduce the clinker factor [2]. This has accelerated the adoption of blended cements that incorporate supplementary cementitious materials (SCMs) by replacing part of the Portland cement (OPC) fraction. Among commonly used SCMs are fine limestone, granulated blast furnace slag and fly ash [3]. However, fly ash and slag are combined available quantities close to 15% of the cement production [4]. In the case of fly ash, the availability is expected to decrease as more thermal power plants are converted to use cleaner fuels [2]. This means that we need to look for other materials to further reduce clinker factor, such as calcined clays.

Limestone calcined clay cements (LC^3) are one of the promising alternatives for high performance sustainable cements [5–7]. LC^3 incorporates significant amounts of metakaolin, a reactive aluminosilicate phase [8] formed after calcination of kaolinitic clays, and ground limestone ($CaCO_3$). Both materials are widely available and therefore are suitable to face the current shortage of SCMs [2]. Previous studies have focused on different stages of the processing of calcined clays, such as grinding [9–11] and colour control [12]. In addition to metakaolin and limestone, an additional amount of gypsum (relative to clinker) is normally required to achieve proper sulfate balance and maximal performance of LC^3. This additional sulfate compensates the acceleration of the aluminate peak due to the "filler effect" of metakaolin and limestone. This filler contribution accelerates the reaction of alite, forming more C-S-H on which sulfate adsorbs, leading to faster sulfate depletion (i.e., the aluminate peak shifts to the left). The optimization of the sulfate addition in LC^3 blends was studied in [13,14].

LC^3 can achieve equivalent strength to OPC at 7 days with a clinker content of only 50% if the kaolinite content of the calcined clay used is above about 40% [6,15]. The high reactivity of metakaolin contributes to achieve a dense microstructure in LC^3 systems at early ages [16], making LC^3 particularly resistant to chloride ingress [17]. A major factor contributing to this good performance is the higher amounts of CO_3-AFm[1] phases, which will be referred as carbo-aluminate phases. These carbo-aluminate phases are hemicarboaluminate ($C_4Ac_{0.5}H_{12}$, Hc) and monocarboaluminate (C_4AcH_{11}, Mc), which are formed in LC^3 systems due to the reaction between metakaolin and limestone [8,16].

In addition to the normal reactions of pure Portland cement, three main reactions occur in LC^3 systems: First is the classic pozzolanic reaction, where metakaolin (AS_2) can react with portlandite (CH) produced during cement hydration to form C–A–S–H [16,18], thus contributing to strength by space filling (Eq. (1)). Second, the alumina in

* Corresponding author.
E-mail address: franco.zunino@epfl.ch (F. Zunino).

[1] AFm (Al_2O_3-Fe_2O_3-mono) denotes a group of layered structure aluminate hydrate phases with general formula $C_4(A,F)X_2{\cdot}yH$, where X represents a unit of a single (OH^-, Cl^-) or half a unit of a double (SO_4^{2-}, CO_3^{2-}) charged anion [28].

https://doi.org/10.1016/j.cemconres.2020.106307
Received 4 August 2020; Received in revised form 2 November 2020; Accepted 10 November 2020
Available online 18 November 2020

Table 1
Chemical (from XRF) and phase composition (from XRD) of OPC, metakaolin, LS and C_3S.

	OPC	Metakaolin (MK)	LS	C_3S
SiO_2	19.511	52.00	0.11	24.11
Al_2O_3	4.42	43.80	0.00	0.00
Fe_2O_3	3.12	0.33	0.04	0.07
CaO	63.85	0.03	54.96	74.57
Na_2O	0.19	0.14	0.06	0.00
K_2O	0.83	0.29	0.00	0.00
MnO	0.05	0.01	0.00	0.00
TiO_2	0.31	1.53	0.00	0.00
MgO	2.10	0.01	0.15	0.15
P_2O_5	0.33	0.16	0.00	0.00
SO_3	3.25	0.10	0.03	0.00
LOI	1.54	1.47	42.5	1.05
C_3S	66.5	–	–	>99.5
C_2S	4.0	–	–	–
C_3A	4.9	–	–	–
C_4AF	9.6	–	–	–
Gyp	6.3			

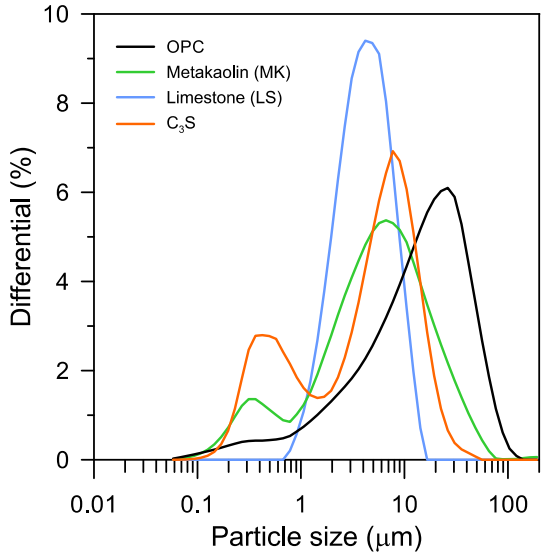

Fig. 1. Particle size distributions of materials used in this study.

the C_3A can react with limestone and portlandite, to form monocarboaluminate and hemicarboaluminate [19,20] instead of monosulphoaluminate ($C_4A\$H_{12}$) as AFm phases, which leaves more sulfates available to form ettringite (Eq. (2)). Third, In LC^3 systems, higher amounts of Hc and Mc are observed compared to systems without metakaolin addition. This is due to the reaction of aluminates from metakaolin with calcium carbonate from limestone, leading to the formation of additional hemicarboaluminate (Eq. (3)).

$$AS_2 + 3CH + 6H \rightarrow C - A - S - H + C_2ASH_8 \quad (1)$$

$$C_3A + 0.5Cc + 0.5CH + 11.5H \rightarrow C_4Ac_{0.5}H_{12} \quad (2)$$

$$AS_2 + 0.5Cc + 3.5CH + 8.5H \rightarrow C_4Ac_{0.5}H_{12} \quad (3)$$

While it is clear that the additional precipitation of CO_3-AFm contributes to space filling [16,18,21], there is a lack of systematic studies that directly relate AFm precipitation with space filling and strength development in LC^3. As carboaluminates are formed in larger amounts in LC^3 systems in comparison to OPC or other blended cements, understanding their contribution to refinement and strength is relevant to optimize the use of these systems. This paper studies the role of the additional formation of hemicarboaluminate and monocarboaluminate from the reaction of metakaolin and limestone on mechanical properties

Table 2
Particle size distribution values, span (width), specific surface area and specific gravity of raw materials.

	OPC	MK	LS	C_3S
D_V90 (μm)	41.42	20.17	7.93	14.5
D_V50 (μm)	14.22	5.13	3.93	4.9
D_V10 (μm)	1.67	0.54	1.80	0.4
Span (−)	2.80	3.83	1.56	2.88
SSA (m^2/g)	1.41	13.56	3.60	2.87
Sp. Gravity (g/cm^3)	3.09	2.20	2.72	3.15

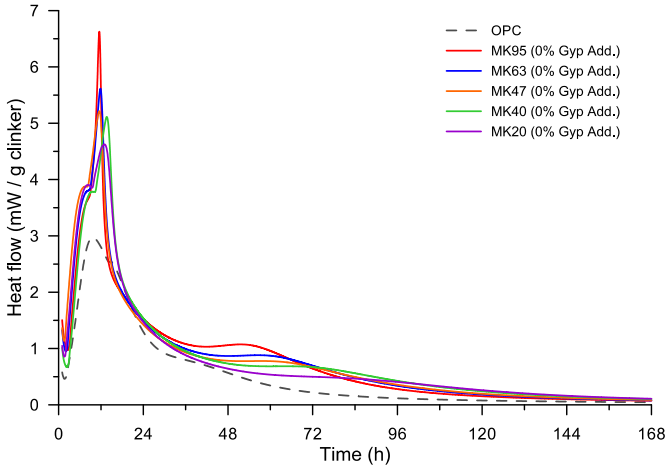

Fig. 2. Heat flow curves of LC^3 systems with different grades of clay, with no additional gypsum incorporated to the system.

and space filling of LC^3 systems. In addition, the kinetics of this reaction are studied, and the effect of different factors that can influence this reaction are presented.

2. Materials and methods

2.1. Materials

A commercial ordinary Portland cement (OPC) conforming to EN 197–1 as CEM I 42.5R was used in this study. The chemical (by XRF) and phase (by XRD / Rietveld) compositions are shown in Table 1. The calcined clay was a high purity metakaolin (MK, 95% purity from Burgess) for simplicity and to avoid possible side effects from secondary materials. A limestone powder with a content of calcium carbonate above 98% as measured by thermogravimetric analysis (TGA) was selected to prepare the LC^3 blends.

To decouple the effect of aluminium contribution from Portland cement (C_3A phase) and metakaolin, some systems were prepared using pure C_3S + LC^2 (combination of limestone, calcined clay and gypsum). The synthesis of pure tricalcium silicate (C_3S) was conducted following the procedure described in [22]. Calcium carbonate (VWR) and fumed silica (0.2 μm, Sigma-Aldrich) were used. The sintering temperature was maintained at 1600 °C for 4 h, and the samples were subsequently quenched in air. The result was triclinic (T_1) C_3S with a free lime content below 0.5% in all batches, as quantified by Rietveld refinement. After synthesis, the C_3S was ground in a concentric disc mill in batches of 100 g with 6, 30 s cycles of grinding with 30 s intervals between them.

The particle size distribution (PSD) of these materials, measured by laser diffraction, is shown in Fig. 1. The optical model parameters and the dispersant were selected following the recommendations given in [23]. A summary of the main size distribution percentiles (D_{V90}, D_{V50} and D_{V10}) and distribution spans ($\frac{D_{V90}-D_{V10}}{D_{V50}}$) is given in Table 2.

The specific surface area (SSA) of each raw material was measured

Table 3
Mixture proportions of OPC, LC^3 and $C_3S + LC^2$ systems.

Mixture	OPC (%)	C_3S (%)	MK (%)	LS (%)	Added Gypsum (%)	w/c	w/b	SSA (m^2/g)
OPC	100	0.0	0.0	0.0	0.0	0.40	0.40	1.41
LC^3 MK95	55-G	0.0	30.0	15.0	G (0 to 12)	0.73[A]	0.40	5.36
LC^3 MK63	55-G	0.0	20.0	25.0	G (0 and 1)	0.73[A]	0.40	4.37
LC^3 MK47	55-G	0.0	15.0	30.0	G (0 and 0.85)	0.73[A]	0.40	3.88
LC^3 MK40	55-G	0.0	12.6	32.4	G (0, and 0.7)	0.73[A]	0.40	3.64
LC^3 MK20	55-G	0.0	6.3	38.7	G (0 and 0.35)	0.73[A]	0.40	3.02
C_3S	0.0	100	0.0	0.0	0.0	0.50	0.50	2.87
$C_3S + LC^2$ MK95	0.0	53.4	30.0	15.0	1.6	0.94	0.50	6.14
$C_3S + LC^2$ MK63	0.0	54.0	20.0	25.0	1.0	0.93	0.50	5.16
$C_3S + LC^2$ MK40	0.0	54.3	12.6	32.4	0.7	0.92	0.50	4.43

[A] Value of w/c computed considering an OPC content of 55%. The value will vary as the concentration of added gypsum is increased.

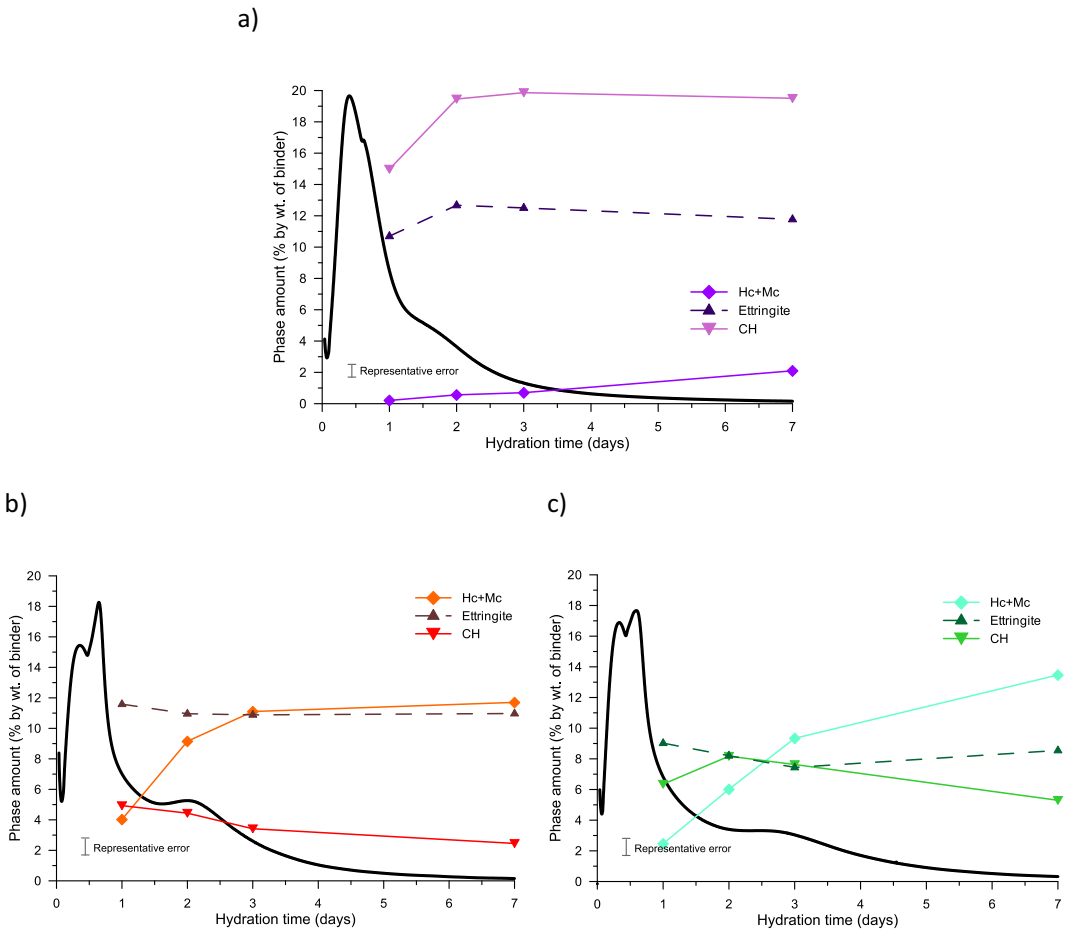

Fig. 3. Phase evolution determined by XRD during the first 7 days of hydration of OPC (a), LC^3 MK95 9 (b) and LC^3 MK40 (c).

by nitrogen adsorption, using the BET model. In all cases, samples of around 1.5 g were degassed for 2 h at 200 °C under a N_2 flux before the measurement. The variability of repeated measurements lies within 5% of the measured value. The specific gravity was measured using a liquid pycnometer with isopropanol as solvent except in the case of C_3S where a helium pycnometer was used instead. Results are shown in Table 2.

2.2. Mixture design

The contribution of the different sources of alumina on the precipitation of hemicarboaluminate and monocarboaluminate was studied by comparing LC^3 systems with equivalent mixtures in which the OPC is replaced by C_3S. The reference LC^3 system contained 55% OPC, 15% limestone and 30% calcined clay (LC^3-50) on a mass basis with an additional amount of gypsum (0 or an optimum content determined by calorimetry in preliminary trials), as shown in Table 3. The calcined clay fraction in LC^3-50 was varied to represent different grades of metakaolin contents in calcined clay. These synthetic clays were prepared by mixing pure MK (95% metakaolin) with limestone, as detailed in Table 3. Following this approach, LC^3 systems with calcined clay MK content ranging from 95% to 20% were prepared. The LC^3 system with 95% metakaolin was studied at a variety of gypsum contents in addition to 0 and the optimum (1.6%). The water-to-binder ratio (w/b) was fixed at 0.4 by mass in all cases.

The synthetic calcined clays with 95, 63 and 40% of metakaolin were selected to further study the formation of hemicarboaluminate and

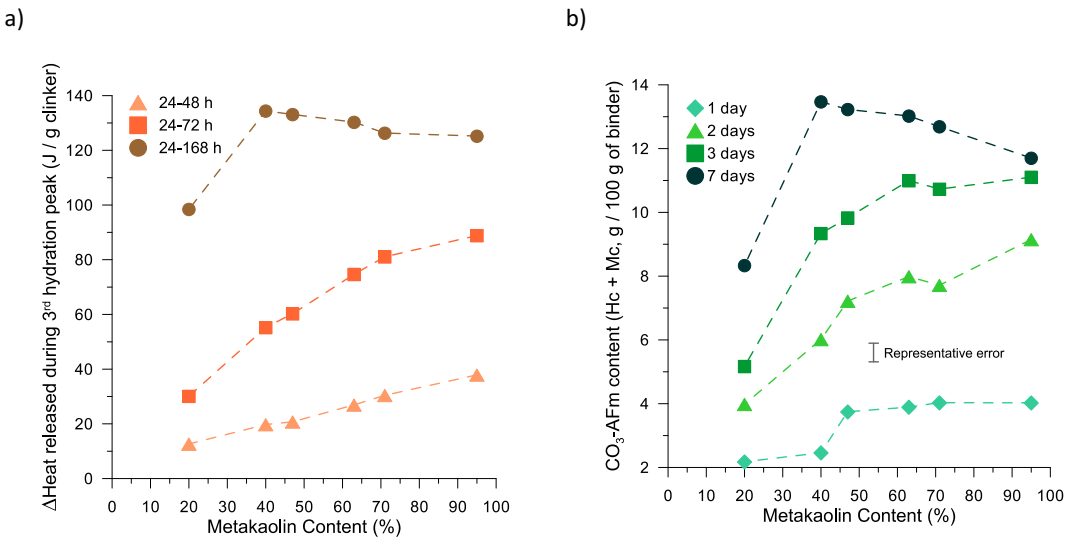

Fig. 4. Heat released during the third hydration peak (a) and evolution of Hc + Mc precipitation vs MK content of LC^3 systems.

monocarboaluminate in C_3S + LC^2 systems. For these mixtures, a w/b ratio of 0.5 by mass was used to achieve sufficient workability with a comparable plasticizer dosage as the OPC-based systems. Gypsum was added to the systems in the same proportion as in the equivalent LC^3 mixtures, in order to keep as many factors as possible constant and isolate the contribution of the metakaolin from the C_3A. The mixture design of these systems is also shown in Table 3.

2.3. Experimental methods

The heat evolution was measured in a TAM Air isothermal calorimeter at 20 °C for up to 7 days. Paste samples were mixed with a high shear mixer at 1600 rpm for 2 min, 10 g of paste were placed in a glass ampoule, sealed and introduced in the calorimeter.

X-ray diffraction (XRD) measurements were carried out on freshly cut slices of hardened paste at 1, 2, 3, 7, 28 and 90 days of hydration to determine the amounts of ettringite, portlandite and carboaluminates formed. Rietveld refinement was conducted using the HighScore Plus v4.8 software. C_3S + LC^2 systems were also characterized by TGA (30 to 1000 °C with a heating ramp of 10 °C/min under N_2) to obtain a second measurement of CH content. The slices were analysed in a Bragg-Brentano configuration by a PANalytical X'pert pro diffractometer operated at 45 kV and 40 mA with a copper source. A 1/2° soller slit was used, and scans were acquired between 7 and 70° 2θ in 14 min, equivalent to a step size of 0.0167° 2θ. The external standard method was used to compute the K-factor of the device and account for the amorphous phases present. A scan of a rutile standard was acquired in the same conditions after the experiments for this purpose.

Porosity measurements were conducted by mercury intrusion porosimetry (MIP) in paste samples at 1, 2, 3 and 7 days. Slices similar to the ones prepared for XRD were immersed in isopropanol (reagent grade, 99% purity) for 7 days to arrest the hydration. Afterwards, they were stored in a desiccator for at least 48 h to remove the remaining isopropanol. About 1 g of hardened paste was placed in a glass dilatometer crushed into 4 to 5 pieces. Intrusion was done up to a pressure of 440 MPa.

In-situ measurements of porosity refinement were conducted on an Ultratest device to measure ultrasonic pulse velocity. Fresh paste samples of LC^3 MK95 and MK40 were placed in a 100 cm^3 capacity ring device mounted over a vibration-reducing table. Two, high-resolution (0.05 μs) ultrasonic cells were placed on opposite sides of the cell, and the pulse velocity was recorded for up to 120 h of hydration at 23 °C.

Mortar samples were prepared following EN 196–1 standard to determine the compressive strength of the LC^3 systems. The binder design was the same as shown in Table 3, and they were combined with standardized sand in a sand-to-binder ratio of 3 by mass. Sealed-curing conditions at 20 °C were applied to the samples until the time of measurement. Measurements were made at 1, 2, 3, 7, 28 and 90 days.

The microstructural development was studied using scanning electron microscopy (SEM) on a FEI Quanta 200 microscope. Element distribution maps were collected from polished sections of LC^3 paste (from the similar discs as for MIP measurements) embedded in resin, using an accelerating voltage of 12 kV, a working distance of 12.5 mm and a spot size adjusted to obtain about 0.9 nA of current over the sample. The maps were collected at 1000× magnification in 30 scans with a dwell time of 512 μs, resulting in a total measuring time of approximately 8 h per map. The data obtained was then quantified using a calibration database acquired under the same conditions. Afterwards, the *edxia* image analysis framework was used to process the hyperspectral maps and obtain phase distribution masks [24].

3. Results and discussion

3.1. The third peak of hydration in LC^3 cements

The series of heat flow curves of LC^3 systems with different metakaolin contents is shown in Fig. 2, without additional gypsum. This is intended to decouple the contribution of metakaolin content and sulfate content (discussed in Section 3.7.1).

The alite (first)[2] peak occurs after the end of the induction period; it is associated with a fast dissolution of C_3S and precipitation of C-(A)-S-H. Sulfate will be absorbed on this C-(A)-S-H [25]. Ettringite also continues to form slowly during this time. The alite peak of LC^3 appears enhanced as compared to OPC due to the filler effect of limestone and metakaolin [18]. In [13], it was shown that this enhancement influences the sulfate balance of LC^3 systems. Consequently, the sulfate content of LC^3 systems should be adjusted so that the aluminate (second) peak occurs after the alite peak when solid gypsum is depleted. This aluminate (second) peak corresponds to the fast dissolution of C_3A and precipitation of ettringite from the desorption of sulfate from C-(A)-S-H

[2] The dissolution peak observed during the first minutes of hydration is sometimes referred as the first hydration peak. In this work, this dissolution peak is not considered, and consequently peaks are counted starting from the alite peak.

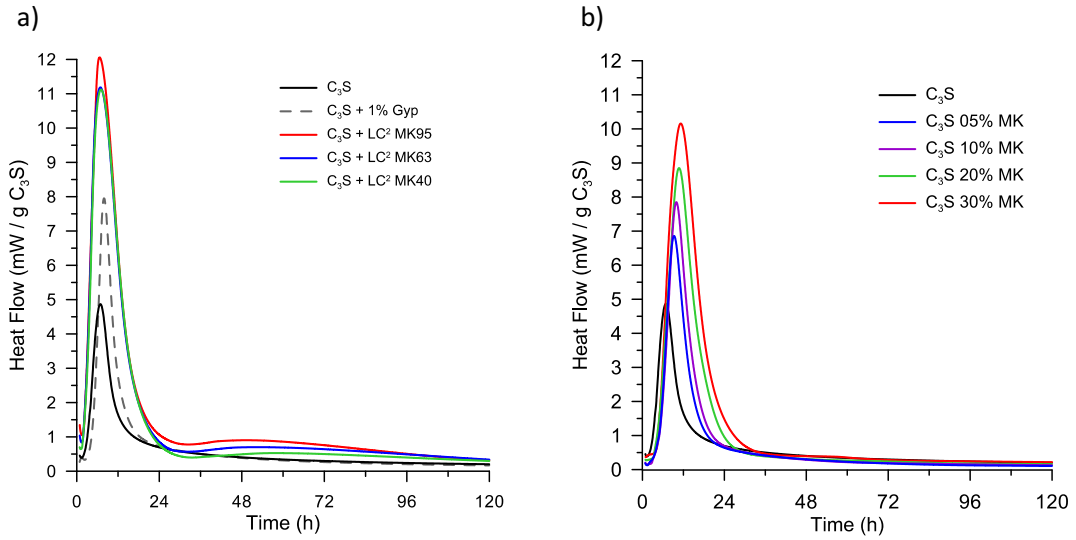

Fig. 5. Heat flow curves of C_3S, C_3S + 1% gypsum and C_3S + LC^2 systems with MK95, MK63 and MK40 clay grades (a) and C_3S with different additions of MK (b).

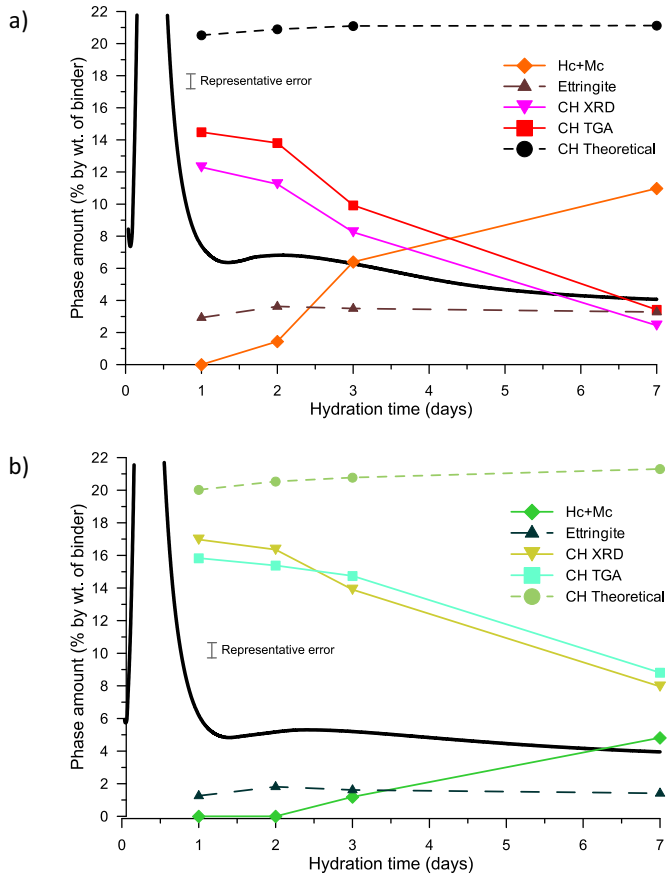

Fig. 6. Evolution of ettringite, portlandite and Hc + Mc precipitation in C_3S + LC^2 systems with MK95 (a) and MK40 (b) clay grades.

[25,26].

A third hydration peak (considering the alite peak as the first) is observed in LC^3 systems, with a maximum between 48 and 72 h of hydration. This third hydration peak is significantly larger than the one observed in OPC following the aluminate peak, which is normally associated with formation of AFm phases. As observed in Fig. 2, the metakaolin content has a strong effect on the position and intensity of this third peak. In the MK95 system, the peak maximizes after about 54 h. In the MK20 system, the peak reaches its maximum after 86 h of hydration.

Fig. 3 shows the evolution of CH, Ett and Hc/Mc obtained from XRD for OPC, LC^3 MK95 and MK40 during the first 7 days of hydration (for diffraction patterns see Fig. A1 in appendix). Hc and Mc are observed in low amounts in the LC^3 systems at 24 h, while in OPC, peaks of these phases are not significant until 7 days of hydration. Both LC^3 and OPC form Hc and Mc as AFm phases, as OPC contains about 3% limestone. Between 2 and 3 days, the amounts of Hc and Mc increase significantly in the LC^3 systems, more in MK95 than the MK40 system. The amount of CH decreases over time in LC^3 systems, as it is consumed by the pozzolanic reaction of metakaolin. The ettringite content decreases slightly over time, but much remains as it is stabilized by the presence of calcite and the consequent formation of carboaluminates [18].

3.2. *Correlation of heat released during the third hydration peak and Hc/Mc formation*

The total heat released during the third hydration peak was estimated as the total heat gain in the time intervals between 24–48 h, 24–72 h and 24–168 h. The heat contribution of OPC was approximated and subtracted using a curve of an OPC + 20% gypsum (without aluminate and AFm peaks visible) using an analogue procedure as the one shown in [13] for the aluminate peak. This approach does not provide an exact computation of the heat release associated with the third peak, but rather an estimation referred to a common baseline. The computed values are shown in Fig. 4a, for each MK content. Between 1 and 3 days, more heat is released during the third peak as the metakaolin content increases. At 7 days, the highest heat release is seen for the MK40 systems.

Quantification of Hc and Mc by XRD (Fig. 4b) shows that between 1 and 3 days of hydration, more carboaluminates are precipitated as the metakaolin content increase. Afterwards, the highest amount of Hc and Mc is observed in the MK40 system, with decreasing amounts of CO_3-AFm measured as the metakaolin content increases. For the system with MK20, the Hc + Mc content is significantly lower at all ages. The heat release during the third hydration peak (Fig. 4a) and the quantified Hc + Mc amounts by XRD (Fig. 4b) trends are in general agreement. The observed change in trend over time will be further discussed in Section 3.5.

To further investigate the higher amounts of Hc and Mc formed in LC^3 systems, the aluminium source that sustain this reaction should be

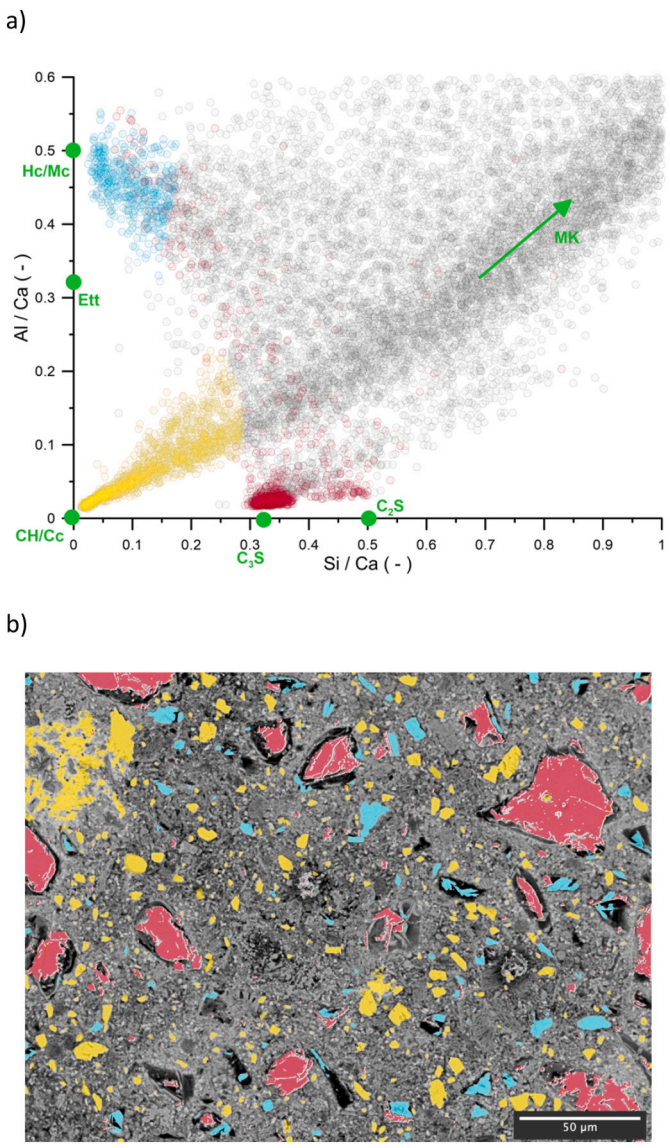

Fig. 7. Al/Ca vs Si/Ca diagram obtained from EDS data collected from the sample of the LC^3 MK95 system at 3 days with composition of main hydrates highlighted with green dots (composition towards MK shown as a green arrow) (a) and masks of CH/Cc, AFm and anhydrous clusters shown overlapped to the BSE micrograph (b). Portlandite + limestone in yellow, Hc + Mc in cyan, anhydrous cement grains in red. (For interpretation of the references to colour in this figure legend, the reader is referred to the web version of this article.)

identified. As the amount of ettringite remains fairly constant up to 90 days, the only possibilities are unreacted C_3A and/or metakaolin.

3.3. The aluminium source for Hc/Mc formation during the third hydration peak

To isolate the contribution of the alumina originating from MK rather than the C_3A of the clinker component, $C_3S + LC^2$ systems were studied. In these materials, aluminium can only come from metakaolin. In Fig. 5a, the heat flow curves of $C_3S + LC^2$ with MK95, MK63 and MK40 are shown and compared to pure C_3S and C_3S + 1% gypsum. The enhancement of the main hydration peak seen in the $C_3S + LC^2$ systems is a combination of the effects of gypsum enhancement on C_3S hydration [14] and the filler effect contribution of limestone and metakaolin.

A peak with maximum between 48 and 72 h is observed in all the $C_3S + LC^2$ systems. The intensity and the position of the maximum heat flow is dependent on the amount of MK as in the OPC-based LC^3 systems (Fig. 2). This peak is not observed in C_3S + MK blends (Fig. 5b) without limestone, indicating that both limestone and metakaolin are involved in this reaction.

To study the phase assemblage of the systems during this peak, XRD analysis and Rietveld refinement up to 7 days of hydration was conducted for both $C_3S + LC^2$ MK95 and MK40. Fig. 6 shows the computed amounts of ettringite, Hc + Mc and CH. Measurements of CH by TGA are also presented, along with a theoretical computation of the CH produced by the system based on the DoH of C_3S. The measured CH values by both techniques are similar and follow the same trend. The difference between the CH produced by C_3S hydration and the measured ones indicates that at as early as 24 h, there is some pozzolanic reaction taking place. The extent of CH consumption is proportional to the metakaolin content of the system during the first 7 days of hydration.

Hc/Mc is not detected at 24 h in either $C_3S + LC^2$ systems. In the system with higher MK content (MK95), Hc is detected after 2 days of hydration, while it is not observed in the system with lower metakaolin content (MK40). At 3 days, Hc is detected in both systems. This trend follows the corresponding positions of the peaks shown in Fig. 5 for these systems.

In the LC^3 systems, Hc is observed after 24 h of hydration (Fig. 3). This suggests that in LC^3 systems, some aluminates from C_3A can participate in the precipitation of AFm after depletion of solid gypsum, and later on (during the third peak), metakaolin contributes the aluminium required for this reaction. This is not the case in $C_3S + LC^2$ systems where C_3A is not present, and thus carboaluminate phases are not detected at 24 h. More Mc is observed in $C_3S + LC^2$ systems relative to Hc as compared to the corresponding LC^3 systems at later ages. This suggests that the pH of the pore solution might play a role in the formation of one or another type of CO_3-AFm phases [27]. In OPC-based systems, pH will be slightly higher due to the presence of minor amounts of alkalis.

As observed in Fig. 6, ettringite is detected in both cases after 1 day of hydration. This indicates that during the first 24 h of hydration, alumina from MK is available to form ettringite if sulfate ions are also available. The ettringite content is higher in the MK95 system as a higher amount of sulfate was added to this system.

Both limestone and metakaolin contribute to the reaction that causes the third hydration peak (Fig. 5), forming Hc and Mc (Fig. 6). Consequently, the third hydration peak observed in these systems corresponds to the reaction shown in Eq. 3.

3.4. Formation of carbo-aluminates in the microstructure

SEM-EDS analysis was used to identify the precipitation of Hc and Mc in the microstructure of LC^3 pastes. The systems MK95 and MK40 were selected as the difference in the position of the third peak between them is sufficiently large enough to be able to track the effect of this reaction in the microstructure. Elemental composition maps were collected for samples hydrated for 1, 3 and 7 days for both systems. Processing of the data was conducted using *edxia* to obtain the data points in an Al/Ca versus Si/Ca diagram, as shown in Fig. 7a. In the plot, the points corresponding to Hc/Mc have been highlighted along with CH/Calcite and anhydrous cement grains. Points close to ettringite composition were not observed indicating that it is intimately mixed with C-A-S-H. Several points corresponding to intermix of metakaolin and AFm are observed. The histogram of the BSE dataset was used to clearly identify points corresponding to anhydrous C_3A and C_4AF, as they appear mixed with carbo-aluminate points. Edxia also allows to create masks from clusters of points that are identified to correspond to a certain phase, as shown in Fig. 7b.

Masks for Hc/Mc were created for each map, and superimposed to the BSE image. The micrographs with highlighted CO_3-AFm clusters are shown in Fig. 8. Precipitation of CO_3-AFm takes place in large pores that remain after OPC hydration, mostly in so called “Hadley grains”. At 1

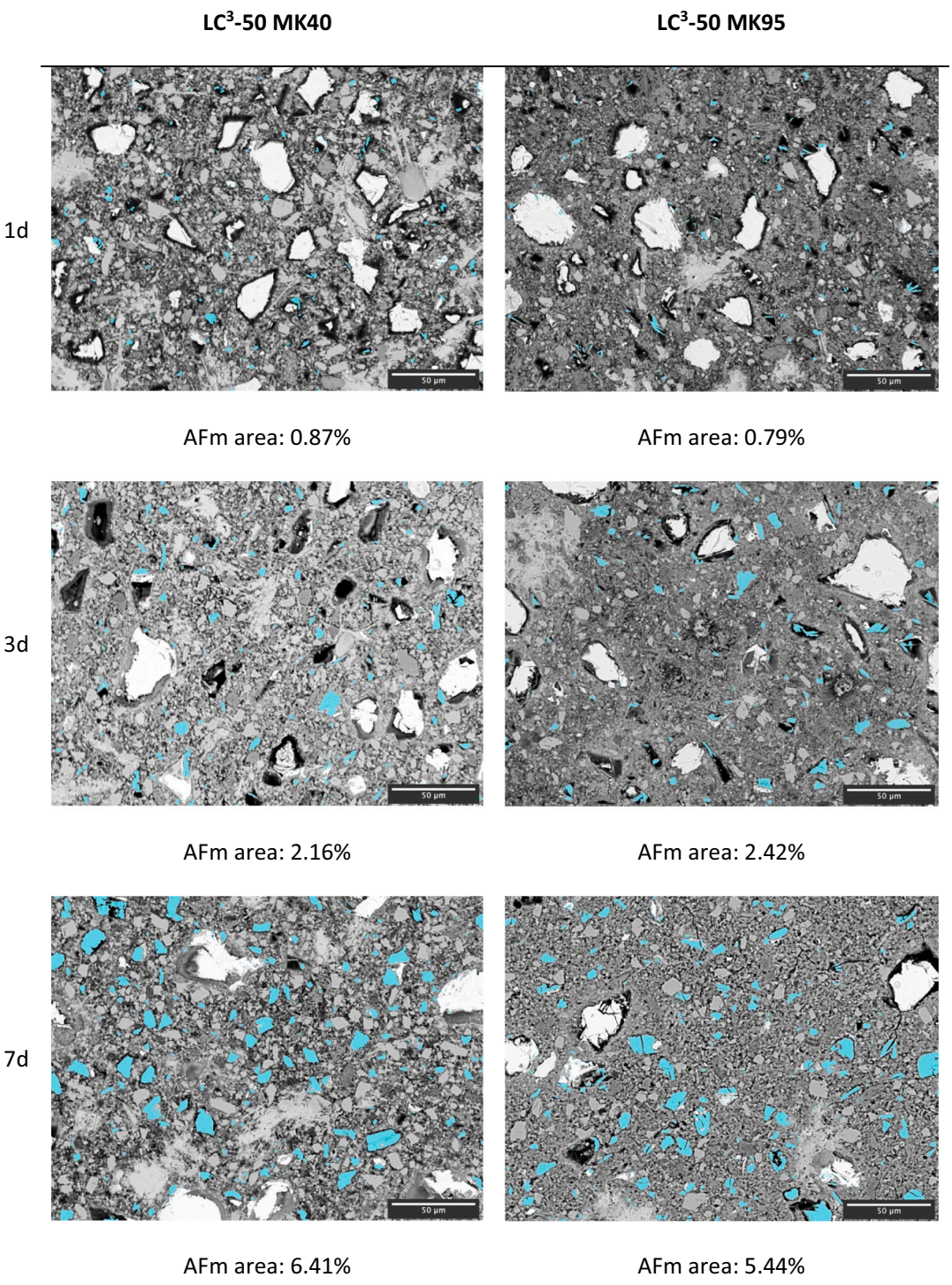

Fig. 8. BSE maps of MK95 and MK40 systems at 1, 3 and 7 days with CO_3-AFm phase highlighted in cyan. (For interpretation of the references to colour in this figure legend, the reader is referred to the web version of this article.)

and 3 days, the distribution of Hc/Mc clusters is very similar between MK95 and MK40 systems. However, at 7 days more AFm is observed in the MK40 sample, in good agreement with XRD results (Fig. 4b). The microstructure of MK95 appears more compact and the porosity more refined at this age. Surface area fractions of the AFm clusters were computed in each case based on the masks generated and are shown alongside each micrograph.

Higher resolution micrographs show the Hc/Mc grains with surrounding C-A-S-H, Fig. 9. Ettringite is highly intermixed with C-A-S-H. This explains the absence of points around the ettringite composition in Fig. 7a due to interaction volume effects. Unreacted metakaolin particles are also observed within the C-A-S-H matrix, explaining the high degree of scatter observed in the point representation for Al/Ca above 0.3.

3.5. The relationship between Hc and Mc precipitation and porosity refinement

A previous study showed that higher amounts of Hc and Mc are

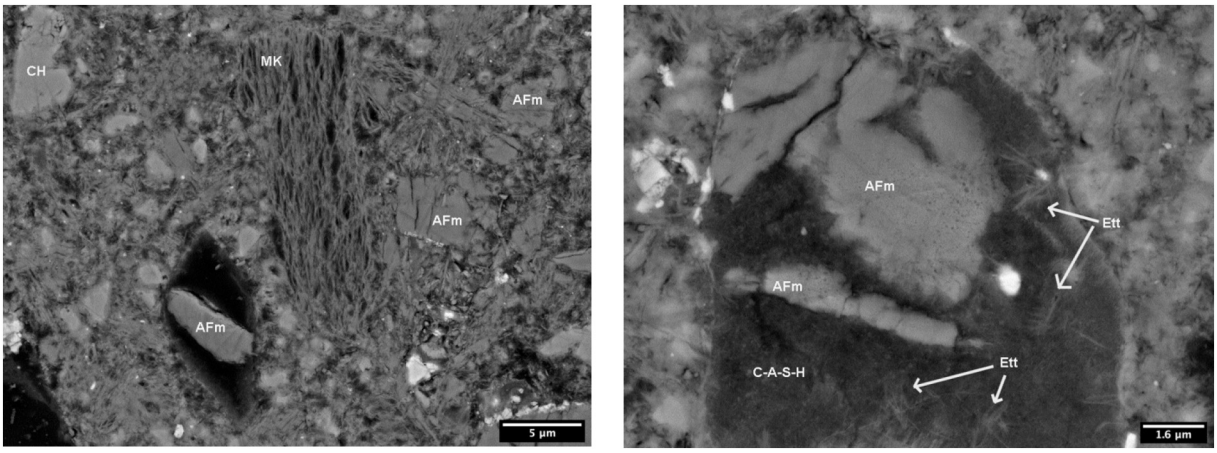

Fig. 9. BSE micrographs of LC^3 MK95 hydrated for 3 days, showing grains of AFm blending with the surrounding C-A-S-H matrix.

observed in LC^3 systems with medium-metakaolin content (40–60%) calcined clays at later ages [16]. In this study, it was proposed that the precipitation of Hc and Mc is limited in the systems with higher MK content calcined clays due to the lack of capillary pores above a critical size. In this case, precipitation becomes more difficult due to the higher supersaturation level required. This could also explain why the systems with 40% MK show the highest amount of Hc/Mc at 7 days of hydration (Section 3.2, Fig. 4).

Fig. 10 shows the total porosity measured by MIP for different LC^3 systems at 1, 2, 3 and 7 days. Results are presented as total porosity versus applied pressure (in MPa), as both are measured magnitudes during the test. The computed pore entry diameter depends on the

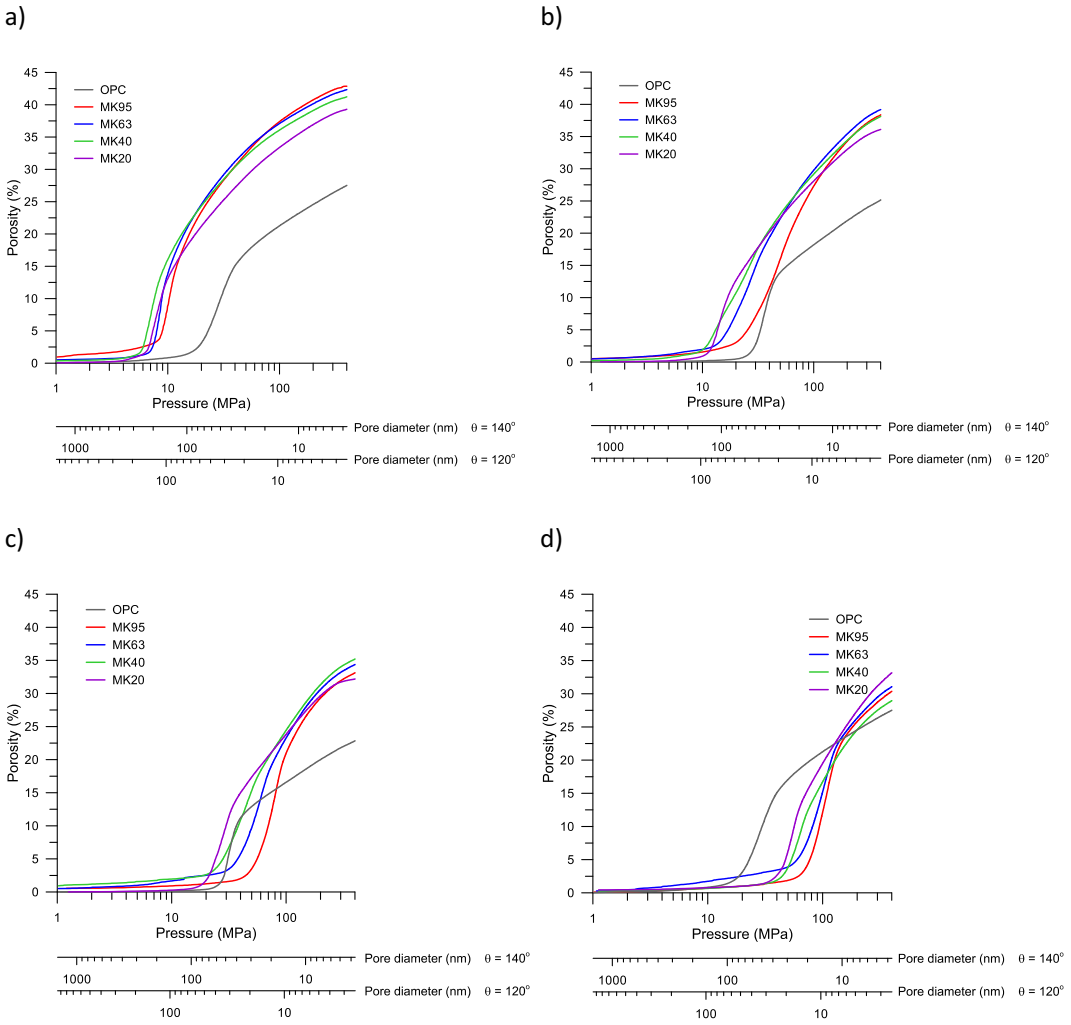

Fig. 10. Total porosity versus applied pressure measured by MIP on OPC and LC^3 systems with different grades of clay after 1 (a), 2 (b), 3 (c) and 7 (d) days of hydration.

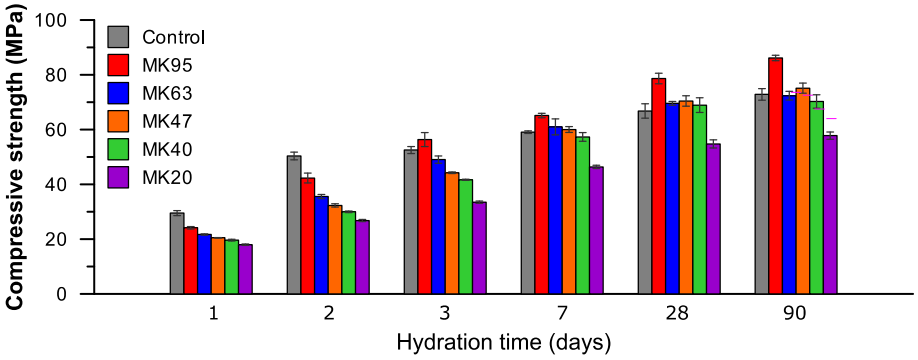

Fig. 11. Compressive strength of LC^3 systems with different grades of clay.

contact angle chosen for the calculations. In this case, two values (120° and 140°, both typically reported in the literature) are presented as additional horizontal axes. The critical entry size can be observed as the point where the slope of the total porosity profiles is maximum.

At 1 day (Fig. 10a), the critical entry size of all LC^3 systems is similar, and significantly larger than OPC. At 2 days (Fig. 10b), the critical pore entry of the MK95 system has significantly reduced, due to an earlier formation of Hc and Mc in this system. At 3 days (Fig. 10c), the critical entry size of MK95 and MK63 is smaller than OPC, while MK40 and MK20 further reduce and start to approach it. Finally, at 7 days (Fig. 10d) all systems exhibit smaller critical entry pore size compared to OPC. The refinement of MK95 is marginal between 3 and 7 days, while the other systems evolve significantly.

Systems with high MK content precipitate CO_3-AFm faster and consequently refine their porosity earlier. The earlier refinement of these high-grade systems limits the additional amount of Hc and Mc that can be precipitated, as seen in Fig. 4. On the other hand, systems with less MK exhibit a coarser porosity in the beginning due to a slower CO_3-AFm formation; and consequently, more space is available for Hc and Mc precipitation at later ages. Therefore, porosity refinement and the precipitation of Hc and Mc in LC^3 systems are intimately related.

3.6. The influence of Hc and Mc precipitation on mechanical properties

The compressive strength results are presented in Fig. 11. At 1 day, the strengths are relatively similar among the LC^3 systems amounts of MK and lower than plain OPC. Strength depends mainly on OPC hydration at this point, and the differences can be attributed to different kinetics of alite hydration due to the filler effect of different amounts of fine MK (see Table 3). At 2 and 3 days, a clear dependence of compressive strength on the metakaolin content of the system is observed. This agrees with a previous study that established metakaolin content as the main parameter controlling LC^3 strength [16]. From 7 days onwards, the situation changes, and the relationship between metakaolin content and strength is less obvious, especially in systems with MK content above 40% where similar strengths are observed. This observation was also made in [16], where a loss of linearity in the strength-metakaolin content correlation was observed at later ages.

As it was discussed in Section 3.1, metakaolin content has an effect in the kinetics of the reaction of metakaolin and limestone that leads to the formation of CO_3-AFm. In addition, this reaction occurs mainly between 2 and 4 days of hydration, depending on the MK content (earlier for higher metakaolin content). This suggests that the precipitation of Hc and Mc associated with the third peak observed in LC^3 systems is responsible for the strength increase observed at these ages. At 7 days, the third hydration peak already occurred in all systems, and as a consequence the strengths become more similar with different amounts of MK. The MK20 system remains lower since the reaction is limited by metakaolin availability.

To further explore this hypothesis, an in-situ measurement of ultrasonic pulse velocity was carried out for the MK95 and MK40 systems. An increase in pulse velocity is normally associated with a reduction of the pore volume and increase in strength. As seen in Fig. 12, a clear split between the two systems occurs at the time of the third peak of the MK95 system, indicating that precipitation of CO_3-AFm indeed leads to a measurable reduction in porosity and to the observed increase in strength. This split takes place at almost the same time when the corresponding calorimetry curves (measured at 23 °C for comparison between both techniques) of MK95 and MK40 diverge due to the earlier occurrence of the third peak in the MK95 system. Later on, the third peak

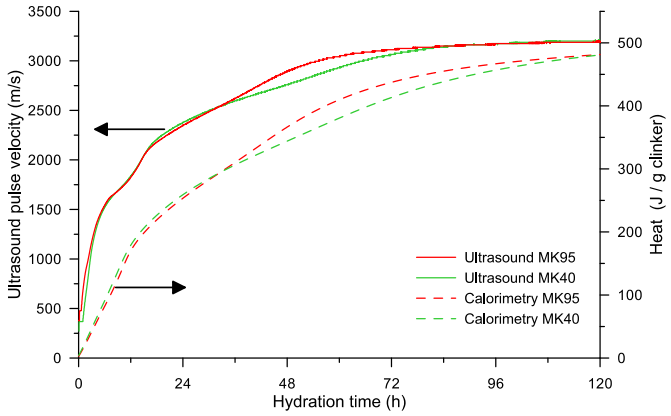

Fig. 12. In-situ ultrasound pulse velocity measured on LC^3 MK95 and MK40 systems. Calorimetry curves of the same systems included for comparison.

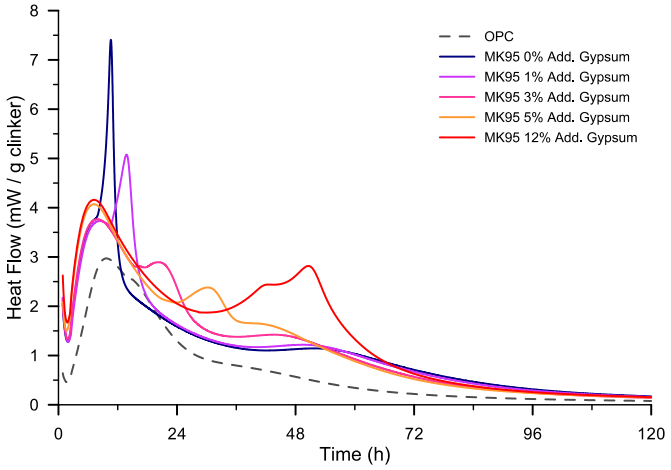

Fig. 13. Heat flow curves of LC^3 MK95 with different amounts of gypsum additions.

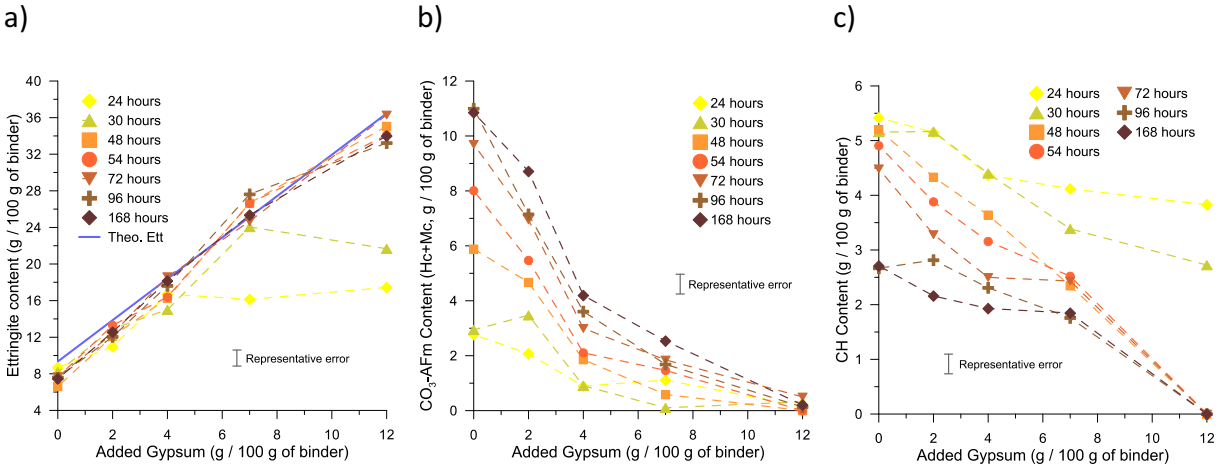

Fig. 14. Ettringite (a), Hc + Mc (b) and portlandite (c) content of LC^3 MK95 system in time with different amounts of gypsum additions.

of the MK40 system takes place and catches up with the MK95 system. This is consistently seen in both pulse velocity and calorimetry measurements. This further supports the relationship between porosity refinement and hydration kinetics, as previously discussed.

3.7. Other factors influencing the reaction of metakaolin and limestone

3.7.1. Influence of sulfate content

The influence of the sulfate content on the reaction of metakaolin and limestone in LC^3 was studied in the LC^3 MK95 system, with added gypsum contents varying from 0 to 12% by mass of binder. The heat flow curves of these systems are shown in Fig. 13. As the sulfate content increases, the onset of the aluminate (second) peak shifts to the right and becomes broader. The third hydration peak, associated with the reaction of metakaolin and limestone, is enhanced and shifted slightly to the left with increasing gypsum addition. At contents of 5 and 12% of added gypsum, the second and third peaks appear to partially overlap.

XRD analysis was conducted in these systems to observe possible changes in the phase assemblage due to the addition of larger amounts of sulfate. Phase quantification obtained by Rietveld refinement for ettringite, Hc + Mc and CH contents are shown in Fig. 14 a, b and c respectively. In the case of ettringite, a theoretical line of ettringite content is included, assuming that all SO_3 participates in ettringite formation.

The ettringite content increases steadily with the increase in gypsum content of the system. This indicates that the alumina from metakaolin participates in the formation of additional ettringite until gypsum is depleted, as the amounts are well above the potential formation of alumina from C_3A only. Furthermore, the ettringite content approaches the expected values assuming that all sulfate available is consumed in ettringite precipitation. The increase in ettringite content is accompanied by a decrease in the Hc + Mc content, Fig. 14b.

In normal OPC systems, alumina from C_3A reacts with sulfate to form ettringite during the first hours of hydration. From a stoichiometry point of view, C_3A and gypsum provide enough calcium to sustain this ettringite formation. When ettringite is formed with aluminates from metakaolin the situation is different, as metakaolin does not contain calcium. However, ettringite still forms as seen in Fig. 14a, indicating that calcium comes from the alite hydration via the pore solution. Fig. 14c shows that the amount of CH decreases significantly as the amount of gypsum is increased in the system, reaching even complete depletion at 7 days for a 12% gypsum addition.

3.7.2. Water-to-binder ratio

As discussed in the previous sections, porosity refinement has an effect on the reaction kinetics of metakaolin. The effect of initial space

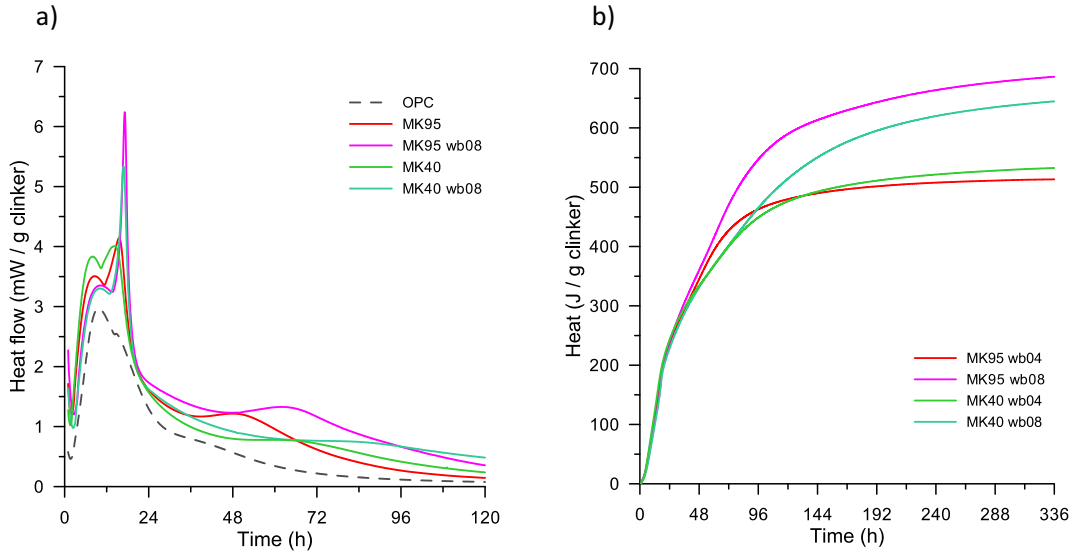

Fig. 15. Heat flow (a) and total heat (b) of LC^3 MK 95 and MK40 with w/b ratio of 0.4 and 0.8.

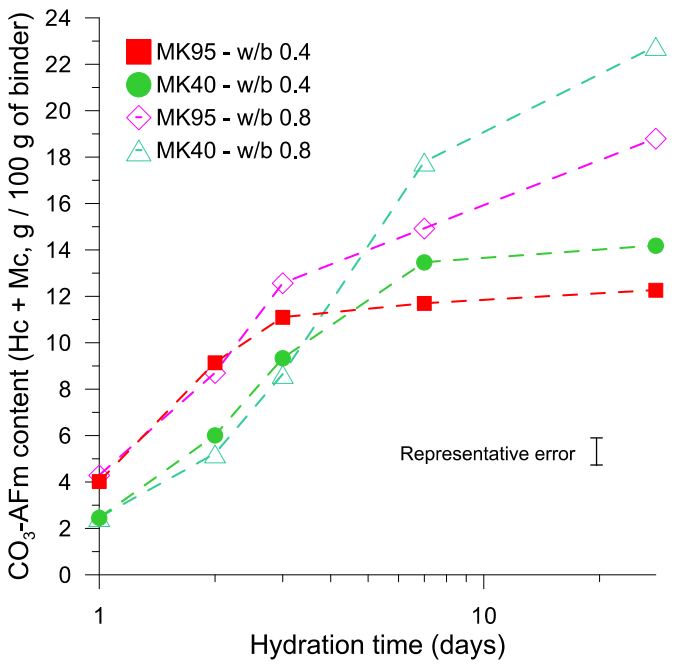

Fig. 16. Hc + Mc content over time in low and high w/b ratio LC^3 systems.

was further studied by increasing the w/b ratio of MK95 and MK40 systems to 0.8. It should be noted that no bleeding was observed in the high w/b systems. The heat flow and total heat curves are shown in Fig. 15.

The aluminate (second) peak of both LC^3 systems appears enhanced in the w/b 0.8 systems as compared to w/b 0.4. However, the position of the onset of the peaks is slightly retarded in the high w/b systems, which can be explained by the lower alite peak observed [13]. The corresponding third peaks appear retarded in the w/b 0.8 systems.

The total heat curves shown in Fig. 15b present some additional insights regarding the hydration of LC^3 systems. Up to about 48 h for MK95 and 80 h for MK40, the systems at high and low w/b exhibit similar total heat release (Fig. 15b). This shows that despite the enhancement of the aluminate (second) peak, the extent of the reaction is similar among corresponding high and low w/b systems, as they contain the same amount of sulfate.

After 48 h, a split occurs between the corresponding high and low w/b systems. The low w/b systems slow down while the high w/b ratio systems continue at a high rate of reaction for a longer period of time. The time when the curve splitting occurs matches relatively well with the position of the maximum of the third peak of hydration in the low w/b systems. As seen in Fig. 10, at this time the corresponding systems reach a high degree of porosity refinement due to the precipitation of carboaluminates. The match between the third peak of hydration in LC^3 and the split point of the curves with high and low w/b provide further evidence of the relationship between the deceleration of the reaction and the precipitation of Hc and Mc.

Fig. 16 shows the carboaluminate content of high and low w/b ratio systems between 1 and 28 days of hydration. Similar contents of Hc/Mc are observed at high and low w/b for up to 2 days of hydration on each system. Afterwards, splitting occurs at times comparable to the observation based on calorimetry measurements (Fig. 15b), and higher carboaluminate contents are observed in the high w/b ratio systems from this point onwards. This shows that space availability influences the precipitation of Hc and Mc and consequently, the heat released during the third hydration peak. After 28 days of hydration, the MK40 system at w/b 0.8 has the highest content of carboaluminates.

4. Conclusions

In this paper, the reaction of metakaolin and limestone was studied, and its effects on porosity refinement and mechanical properties were assessed. In LC^3-type cements, the content of alumina is significantly higher than in conventional OPC. Aluminate hydrates play an important role in the hydration and properties of this systems.

Based on the results presented, the following conclusions can be drawn:

1. The third peak of hydration observed in LC^3 cements corresponds to a precipitation of hemicarboaluminate and monocarboaluminate from the reaction of metakaolin and limestone. The heat released during this peak can explain the trends observed in Hc and Mc precipitation.
2. The precipitation of Hc and Mc is responsible for the rapid porosity refinement observed in LC^3 at early ages that leads to a deceleration of the reaction rate of metakaolin. At 7 days, the observed amounts of CO_3-AFm are smaller in LC^3 systems with higher MK content where the refinement takes place earlier.
3. Hemicarboaluminate and monocarboaluminate precipitate in pores left behind by clinker hydration. The clusters of carboaluminates are intermixed with the surrounding C-A-S-H matrix, effectively contributing to porosity refinement and strength development.
4. Metakaolin and sulfate content both affect this third peak of hydration. These factors lead to an earlier occurrence of the peak. An increase in the water to binder ratio of the system causes the peak to reach its maximum later. As more space is available for precipitation of hydrates, the deceleration of the reaction occurs later and higher heat release per gram of OPC are observed at early ages.
5. The alumina from metakaolin can participate in the formation of ettringite until depletion of solid gypsum in the system. This reaction occurs instead of CO_3-AFm precipitation until gypsum is depleted, leading to a reduction in the amounts of Hc and Mc. The precipitation of ettringite requires additional calcium from the system, which comes from portlandite.

Supplementary data to this article can be found online at https://doi.org/10.1016/j.cemconres.2020.106307.

CRediT authorship contribution statement

Franco Zunino: conceptualization, methodology, writing-original draft preparation, writing-reviewing and editing

Karen Scrivener: supervision, writing-reviewing and editing

Declaration of competing interest

The authors declare that they have no known competing financial interests or personal relationships that could have appeared to influence the work reported in this paper.

Acknowledgements

The authors would like to acknowledge financial support by the Swiss Agency of Development and Cooperation (SDC) grant 81026665. The Swiss federal commission for scholarships for foreign students (FCS) is acknowledged for supporting Franco Zunino's studies through scholarship 2016.0719. The authors acknowledge Dr. Hamed Maraghechi for conducting the in-situ ultrasound pulse velocity measurements. Solène Barbontin is also acknowledged for her assistance in the acquisition of high-resolution micrographs, and Maya Harris for proofreading this manuscript.

References

[1] T. Boden, B. Andres, G. Marland, Global CO2 Emissions From Fossil-fuel Burning, Cement Manufacture, and Gas Flaring, 2016.

[2] K.L. Scrivener, V. John, E.M. Gartner, Eco-efficient cements: potential, economically viable solutions for a low-CO2, cement-based materials industry, in: United Nations Environmental Programme (UNEP), 2016.

[3] B. Lothenbach, K. Scrivener, R.D. Hooton, Supplementary cementitious materials, Cem. Concr. Res. 41 (2011) 1244–1256, https://doi.org/10.1016/j.cemconres.2010.12.001.

[4] IEA, CSI, Technology Roadmap: Low-Carbon Transition in the Cement Industry (2018), https://doi.org/10.1007/springerreference_7300.

[5] K. Scrivener, F. Martirena, S. Bishnoi, S. Maity, Calcined clay limestone cements (LC3), Cem. Concr. Res. (2017) 1–8, https://doi.org/10.1016/j.cemconres.2017.08.017.

[6] K. Scrivener, F. Avet, H. Maraghechi, F. Zunino, J. Ston, W. Hanpongpun, et al., Impacting factors and properties of limestone calcined clay cements (LC3), Green Mater. 7 (2019) 3–14, https://doi.org/10.1680/jgrma.18.00029.

[7] F. Zunino, F. Martirena, K. Scrivener, Limestone Calcined Clay Cements (LC3), ACI Mater. J, Submitted, 2020.

[8] M. Antoni, Investigation of Cement Substitution by Combined Addition of Calcined Clays and Limestone, École Polytechnique Fédérale de Lausanne, 2011.

[9] F. Zunino, K. Scrivener, Assessing the effect of alkanolamine grinding aids in limestone calcined clay cements hydration, Constr. Build. Mater. (2020), https://doi.org/10.1016/j.conbuildmat.2020.121293.

[10] F. Zunino, Limestone calcined clay cements (LC3): raw material processing, sulfate balance and hydration kinetics, EPFL Thesis 8173 (2020).

[11] F. Zunino, K. Scrivener, Increasing the kaolinite content of raw clays using particle classification techniques for use as supplementary cementitious materials, Constr. Build. Mater. 244 (2020). doi:https://doi.org/10.1016/j.conbuildmat.2020.118335.

[12] J.F. Martirena Hernández, R. Almenares-Reyes, F. Zunino, A. Alujas-Diaz, K.L. Scrivener, Color control in industrial clay calcination, RILEM Tech. Lett. 5 (2020) 1–7. doi:10.21809/rilemtechlett.2020.107.

[13] F. Zunino, K.L. Scrivener, The influence of the filler effect in the sulfate requirement of blended cements, Cem. Concr. Res. 126 (2019). doi:https://doi.org/10.1016/j.cemconres.2019.105918.

[14] F. Zunino, K. Scrivener, Factors influencing the sulfate balance in pure phase C3S/C3A systems, Cem. Concr. Res. 133 (2020). doi:https://doi.org/10.1016/j.cemconres.2020.106085.

[15] F. Zunino, K. Scrivener, Assessing the effect of calcite impurities in clay on optimal dehydroxylation parameters for enhanced reactivity, in: F. Martirena, A. Favier, K. Scrivener (Eds.), Proc. 2nd Int. Conf. Calcined Clays Sustain. Concr., RILEM Bookseries 16, 2018: pp. 507–513. doi:https://doi.org/10.1007/978-94-024-1207-9_81.

[16] F. Avet, K. Scrivener, Investigation of the calcined kaolinite content on the hydration of limestone calcined clay cement (LC3), Cem. Concr. Res. 107 (2018) 124–135, https://doi.org/10.1016/j.cemconres.2018.02.016.

[17] S. Sui, W. Wilson, F. Georget, H. Maraghechi, H. Kazemi-Kamyab, W. Sun, et al., Quantification methods for chloride binding in Portland cement and limestone systems, Cem. Concr. Res. 125 (2019). doi:https://doi.org/10.1016/j.cemconres.2019.105864.

[18] M. Antoni, J. Rossen, F. Martirena, K. Scrivener, Cement substitution by a combination of metakaolin and limestone, Cem. Concr. Res. 42 (2012) 1579–1589, https://doi.org/10.1016/j.cemconres.2012.09.006.

[19] D.P. Bentz, P.E. Stutzman, F. Zunino, Low-temperature curing strength enhancement in cement-based materials containing limestone powder, Mater. Struct. Constr. 50 (2017). doi:https://doi.org/10.1617/s11527-017-1042-6.

[20] O. Chowaniec, Limestone Addition in Cement. https://infoscience.epfl.ch/record/174700, 2012.

[21] K. Hoang, H. Justnes, M. Geiker, Early age strength increase of fly ash blended cement by a ternary hardening accelerating admixture, Cem. Concr. Res. 81 (2016) 59–69, https://doi.org/10.1016/j.cemconres.2015.11.004.

[22] X. Li, A. Ouzia, K. Scrivener, Laboratory synthesis of C3S on the kilogram scale, Cem. Concr. Res. 108 (2018) 201–207, https://doi.org/10.1016/j.cemconres.2018.03.019.

[23] K. Scrivener, R. Snellings, B. Lothenbach, A Practical Guide to Microstructural Analysis of Cementitious Materials (2016) 540, https://doi.org/10.7693/wl20150205.

[24] F. Georget, W. Wilson, K. Scrivener, edxia: microstructure characterization from quantified SEM-EDS hypermaps, Cem. Concr. Res. Submitted (2020).

[25] A. Quennoz, K.L. Scrivener, Interactions between alite and C3A-gypsum hydrations in model cements, Cem. Concr. Res. 44 (2013) 46–54, https://doi.org/10.1016/j.cemconres.2012.10.018.

[26] K.L. Scrivener, Development of the Microstructure During the Hydration of Portland Cement, University of London, 1984.

[27] A. Mesbah, C. Cau-Dit-Coumes, F. Frizon, F. Leroux, J. Ravaux, G. Renaudin, A new investigation of the Cl–CO32- substitution in AFm phases, J. Am. Ceram. Soc. 94 (2011) 1901–1910, https://doi.org/10.1111/j.1551-2916.2010.04305.x.

[28] Taylor, Cement chemistry, 2nd ed., Thomas Telford, London, 1997.